A Martensite Boundary on the WRC-1992 Diagram

A martensite boundary, based upon magnetic measurements and longitudinal face bend tests, is proposed for the WRC-1992 diagram

BY D. J. KOTECKI

ABSTRACT. The upper martensite boundary line from the Schaeffler diagram for stainless steel weld metals can be transposed to the WRC-1992 diagram. However, magnetic measurements and longitudinal face bend tests of weld metals do not show good correspondence to this boundary. Many deposit compositions of lower chromium and nickel equivalents than those along Schaeffler's transposed martensite boundary show no martensite as-deposited and pass a 2T longitudinal face bend test. Based upon magnetic measurements and bend tests of about 100 weld metal compositions, obtained as single-pass submerged arc deposits on ASTM A36 mild steel, a new martensite boundary is proposed for addition to the WRC-1992 diagram. This boundary separates compositions that exhibit no magnetic response attributable to martensite and pass a 2T longitudinal face bend test from compositions that have magnetic response that indicates the presence of as-deposited martensite and fail the bend test. Because manganese is part of neither the chromium equivalent nor the nickel equivalent on the WRC-1992 diagram, the line is specific to the Mn level considered in the tests — approximately 1% — that is suitable for most stainless steel cladding and dissimilar metal joining situations. It is probably conservative for deposits of much higher Mn content.

Introduction

The WRC-1992 diagram (Ref. 1) for stainless steel weld metals has been recognized by the International Institute of Welding (IIW) as the most accurate and preferred constitution diagram for estimating or predicting ferrite in nominally austenitic and duplex ferritic-austenitic stainless steel weld metals (Ref. 2). As a result, it was incorporated into the ASME *Boiler and Pressure Vessel Code* with its Winter 1994 Addendum. In addition to better predicting accuracy (Ref. 3) than the DeLong diagram (Ref. 4), the WRC-1992 diagram expands the predicting range to 100 FN maximum. However, the much older Schaeffler diagram (Ref. 5), as shown in Fig. 1, continues to be used for predicting ferrite in cladding and dissimilar-metal joining (Ref. 6), in large part because it includes boundaries for martensite appearance in stainless steel weld deposits. In significant quantities, martensite is often undesirable in a stainless steel cladding or in a dissimilar metal joint because its usual low ductility tends to result in fracture during bend testing of the weldment. In these cases, the Schaeffler diagram then provides a tool for selecting filler metal to avoid martensite in the weld metal (Ref. 6).

The Schaeffler diagram makes its predictions in terms of "% ferrite," but there is no reproducible method of determining % ferrite in weld metal. Round robin tests within the Welding Research Council and within Commission II of the IIW showed % ferrite values ranging from 0.6 to 1.6 times the average value (Ref. 7) (*i.e.*, –40% to +60%) for a given sample, which is clearly unacceptable for specifications. On the other hand, in similar round robins, magnetic Ferrite Number measurements showed interlaboratory scatter of ±10% or less (about the average value for a given sample), after calibration of instruments with primary (coating thickness) standards and of ±14% or less after calibration of instruments with secondary (weld-metal-like) standards (Refs. 8, 9). So it is much more attractive to use Ferrite Numbers, rather than "% ferrite," in estimation and prediction of ferrite.

To expand the utility of the WRC-1992 diagram, it is of interest to determine a martensite boundary for that diagram — the objective of the present work. The Schaeffler diagram shown in Fig. 1 contains regions labeled "A + M" and "A + M + F," in which martensite is expected. The regions are bounded above and below by a pair of diagonal lines that proceed from upper left to lower right. It is the upper of these two lines that separates the "Austenite" region from the "A + M" region along the left-most part of the line and separates the "A + F" region from the "A + M + F" region along the right-most part of the line, which is the line of interest. For compositions above this line, no martensite would be expected, while for compositions below this line, some martensite would be expected. It is this line that is termed *Schaeffler's upper martensite boundary*.

KEY WORDS

Martensite
Stainless Steel
Weld Metal
WRC-1992 Diagram
Cladding
Dissimilar Metal Joining

Transposing Schaeffler's Upper Martensite Boundary to the WRC-1992 Diagram

A logical way to begin to develop a martensite boundary for the WRC-1992 diagram is to transpose the boundary from the Schaeffler diagram. However, this is not a straightforward exercise,

D. J. KOTECKI is with The Lincoln Electric Company, Cleveland, Ohio.

because the Schaeffler chromium equivalent (Cr_{eq}) is not the same as the WRC-1992 chromium equivalent, and neither is the Schaeffler nickel equivalent (Ni_{eq}) the same as the WRC-1992 nickel equivalent. These equivalents, in which each element's concentration is given in weight percent (a convention used everywhere herein), are listed below:

Chromium Equivalents

Schaeffler:

% Cr + % Mo + 1.5x(% Si) + 0.5x(% Nb)

WRC-1992:

% Cr + % Mo + 0.7x(% Nb)

Nickel Equivalents

Schaeffler:

% Ni + 30x(% C) + 0.5x(%Mn)

WRC-1992:

% Ni + 35x(% C) + 20x(% N) + 0.25x(% Cu)

Because these equivalents are different, the method of transposing the martensite boundary involves six steps, as follows:

Step 1. Fix the levels of the elements that are different in the two sets of corresponding equivalent values. Since the transposed martensite boundary was to be tested by using single-pass submerged arc deposits, the elements to be fixed were chosen at levels representative of the experimental data that followed. These levels are

C	0.10%
Mn	1.00%
N	0.02%
Mo	0.00%
Si	0.50%
Nb	0.00%

Step 2. Arbitrarily choose two points along Schaeffler's upper martensite boundary. These points are the point where the martensite boundary intersects the Schaeffler 100% ferrite line and the point along the martensite boundary where the nickel equivalent is 15.00%.

Step 3. Use the *Ferrite Predictor* (Ref. 10) computer software to determine the Schaeffler Cr_{eq} and Ni_{eq} corresponding to each of the two arbitrarily chosen points on Schaeffler's upper martensite boundary. Essentially by trial and error with the software, the coordinates of these two arbitrary points on the Schaeffler diagram were found to be

Martensite boundary at 100% ferrite:

Cr_{eq} = 26.205

Ni_{eq} = 4.536

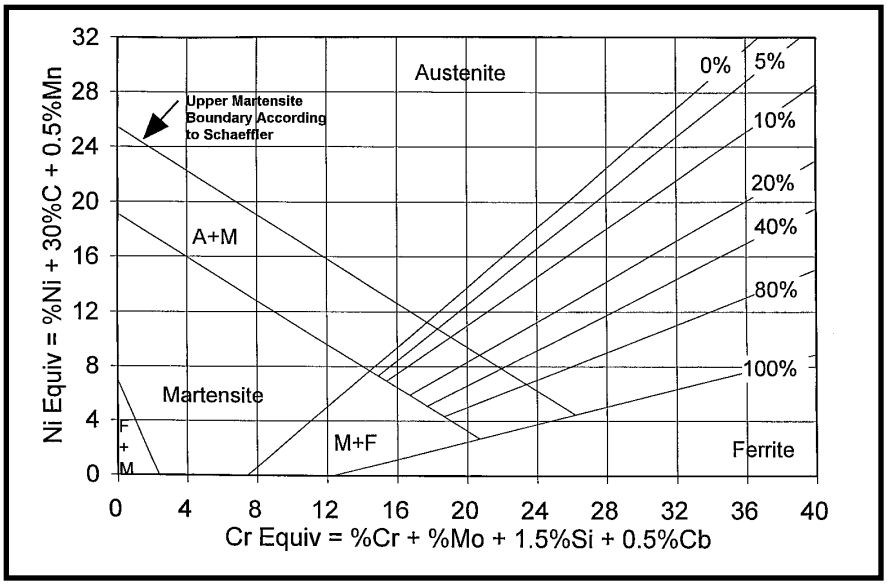

Fig. 1 — Schaeffler diagram.

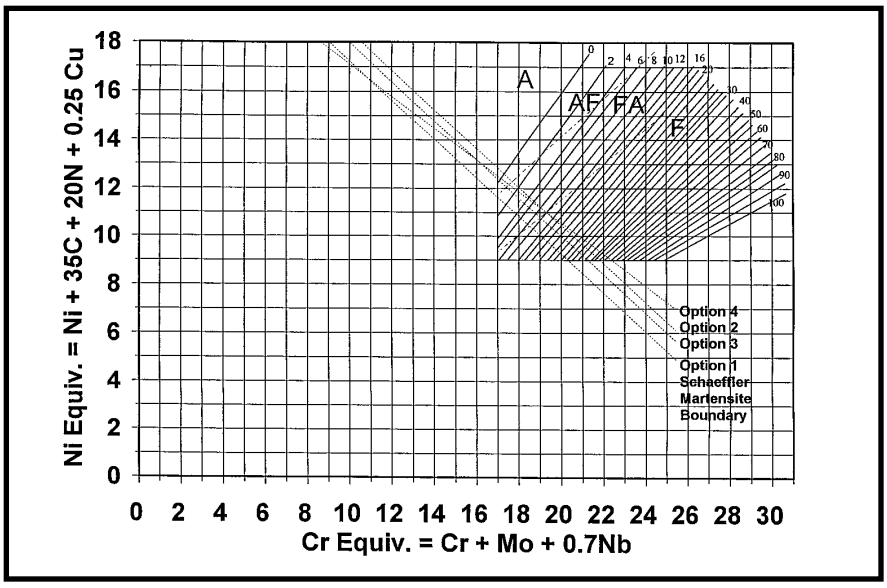

Fig. 2 — WRC-1992 diagram, with four options for upper martensite boundaries transposed from the Schaeffler diagram.

Martensite boundary at 15.00% Ni_{eq}:

Cr_{eq} = 13.046

Ni_{eq} = 15.000

Step 4. Use these two pairs of Cr_{eq} and Ni_{eq} values, with the fixed values for other elements in step 2, to back calculate corresponding % Cr and % Ni levels from the Schaeffler diagram. Calculation of the % Cr corresponding to each of the two chromium equivalents is straightforward. Since Mo and Nb are presumed to be zero, the only operation is to subtract 1.5 times the chosen silicon content from the Schaeffler chromium equivalent from step 3 to find the % Cr

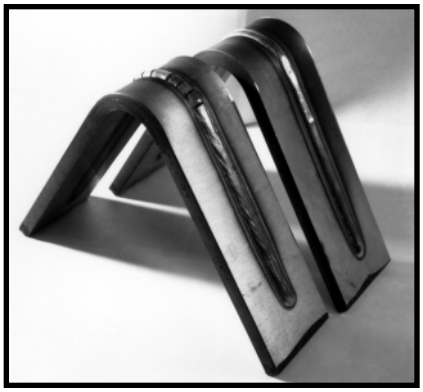

Fig. 3 — Two longitudinal face bend test specimens. The specimen to the rear shows no cracks, while that to the front has numerous cracks.

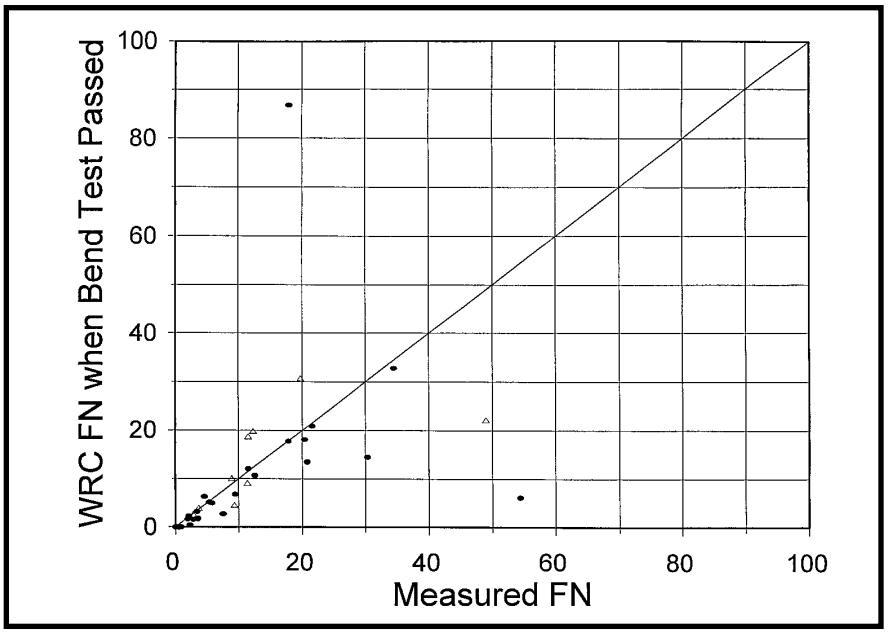

Fig. 4 — WRC FN vs. measured FN (as-deposited) for crack-free bends.

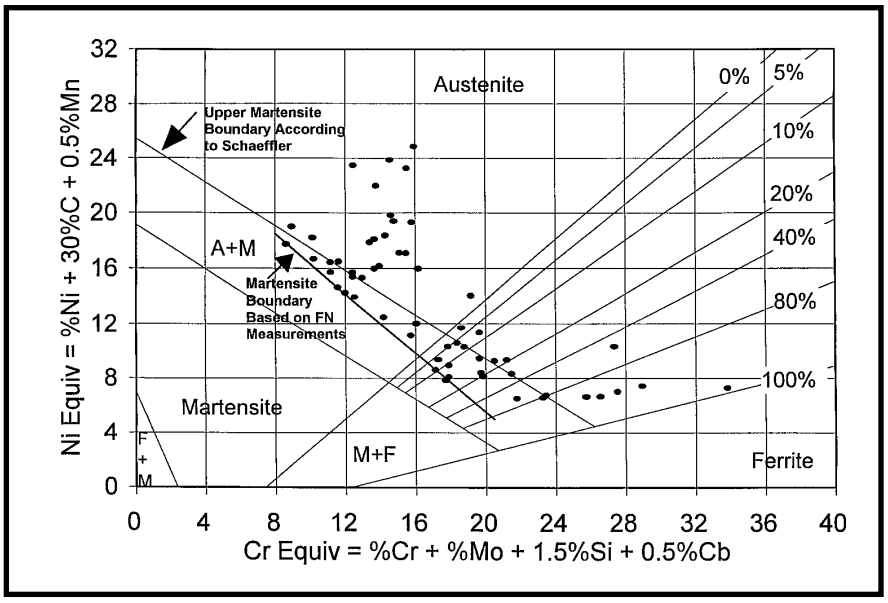

Fig. 5 — Schaeffler diagram, with compositions having measured FN less than 1.0, or having measured FN less than or equal to the WRC-1992 FN + 1, plotted as solid ellipses. No correction for nitrogen is used in plotting these data. The lower limit of these points is taken to be the "martensite boundary based on FN measurements."

Martensite boundary at 100% ferrite:
% Cr = Cr_{eq} – 1.5x(% Si)
= 26.205 – 1.5x(0.5) = 25.455

Martensite boundary at 15.00% Ni_{eq}:
% Cr = Cr_{eq} – 1.5x(% Si)
= 13.046 – 1.5x(0.5) = 12.296

The % Ni calculations offer some options, depending upon how nitrogen is treated. As originally published, the Schaeffler diagram did not consider nitrogen. However, it has been realized that the Schaeffler nickel equivalent can be adjusted for nitrogen.

Option 1. If nitrogen is ignored, the calculations of % Ni for the two arbitrary points are as follows:

Martensite boundary at 100% ferrite:
% Ni = 4.536 – 30x(0.10% C)
– 0.5x(1.0% Mn) = 1.036

Martensite boundary at 15.00% Ni_{eq}:
% Ni = 15.00 – 30x(0.10% C)
– 0.5x(1.0% Mn) = 11.50

Option 2. The Schaeffler diagram is based entirely upon deposited weld metal from covered electrodes. The ASME Code (Ref. 11) indicates a nitrogen content of 0.06% is considered normal. Although not formalized, a common practice is to adjust the Schaeffler nickel equivalent of a weld that departs from this nitrogen value by the factor ΔNi_{eq} given below:

Adjusted Ni_{eq} = Schaeffler Ni_{eq} + ΔNi_{eq}

where ΔNi_{eq} = 30x(% N – 0.06) and where the coefficient 30 is taken from the DeLong diagram (Ref. 4) coefficient for nitrogen. For low nitrogen weld metal, this factor can be negative, and ΔNi_{eq} is –1.20 in the case of the nitrogen content assumed in step 1 above. Applying this approach to find the nickel content at the two arbitrarily chosen points along Schaeffler's upper martensite boundary involves simply subtracting the ΔNi_{eq} from the nickel equivalent from option 1 above, and produces the following:

Martensite boundary at 100% ferrite:
% Ni = 1.036 – ΔNi_{eq}
= 1.036 – (–1.20) = 2.236

Martensite boundary at 15.00% Ni_{eq}:
% Ni = 11.50 – ΔNi_{eq}
= 11.50 – (–1.20) = 12.70

Option 3. Espy (Ref. 12) proposed that Schaeffler's nickel equivalent be modified by adding a different correction factor to it, based upon his experimental data as follows:

Adjusted Ni_{eq} = Schaeffler Ni_{eq} + ΔNi_{eq}

where ΔNi_{eq} = 30x(% N – 0.045) = 30x(0.02 – 0.45) = –0.75 in this case. Applying this approach and subtracting this new ΔNi_{eq} from the Ni_{eq} from option 1 above produces the following:

Martensite boundary at 100% ferrite:
% Ni = 1.036 – ΔNi_{eq}
= 1.036 – (–0.75) = 1.786

Martensite boundary at 15.00% Ni_{eq}:
% Ni = 11.50 – ΔNi_{eq}
= 11.50 – (–0.75) = 12.25

Option 4. Schaeffler provided, in graphical form, a nitrogen correction factor that is dependent upon the chromium content (Ref. 13). This can be reduced to an equation for the actual nitrogen contribution (ΔNi_{eq}) to Schaeffler's nickel equivalent:

ΔNi_{eq} = 30x(Actual % N
–[0.085x%Cr/18 – 0.031%])

At 25.455% Cr, Schaeffler's correction predicts nitrogen of 0.089% and ΔNi_{eq} = –2.07. At 12.296% Cr, Schaeffler's correction predicts nitrogen of 0.027% and ΔNi_{eq} = –0.21. Then new values for % Ni are calculated as

Table1 — Filler Wire Compositions and Ferrite and Representative Base Metal Composition

	C	Mn	P	S	Si	Cr	Ni	Mo	Cu	Nb	N	Measured FN	WRC FN	Schaeffler % Ferrite
Calculated Wire 119	0.07	1.54	0.01	0.01	0.61	19.21	14.84	0.00	0.00	0.00	0.00	N/A	0.0	0.0
Wire 119, Six Layers with 880 Flux	0.06	1.16	0.02	0.01	0.73	19.88	13.40	0.00	0.00	0.00	0.02	0.1	0.0	0.0
Wire 119, 6 Layers with A-100 Flux	0.07	1.71	0.03	0.01	0.74	27.83	12.29	0.03	0.00	0.01	0.04	27.1	31.8	19.1
Measured ER309L	0.02	1.78	0.02	0.01	0.46	24.20	13.95	0.16	0.07	0.02	0.06	N/A	12.2	9.4
Calculated Wire 120	0.07	1.54	0.01	0.01	0.61	19.21	15.64	0.00	0.00	0.00	0.00	N/A	0.0	0.0
Calculated Wire 121	0.07	1.24	0.01	0.01	0.45	14.57	10.92	0.00	0.00	0.00	0.00	N/A	0.0	0.0
Measured ER308L	0.02	1.91	0.02	0.01	0.51	19.54	9.97	0.05	0.02	N/D	0.04	N/A	9.2	8.4
Calculated Wire 65N1693	0.14	2.15	0.03	0.01	0.38	20.12	19.77	0.30	0.20	0.00	0.03	N/A	0.0	0.0
Calculated Wire 65N1694	0.14	2.12	0.02	0.01	0.38	19.69	26.31	0.30	0.20	0.00	0.03	N/A	0.0	0.0
Calculated Wire 65N1695	0.14	2.12	0.03	0.01	0.38	20.12	24.82	0.30	0.20	0.00	0.03	N/A	0.0	0.0
Calculated Wire 65N1716	0.13	1.92	0.02	0.01	0.34	17.61	17.86	0.28	0.20	0.00	0.03	N/A	0.0	0.0
Calculated Wire 65N1717	0.14	1.87	0.02	0.01	0.34	17.61	27.78	0.28	0.20	0.00	0.03	N/A	0.0	0.0
Calculated Wire 65N1743	0.04	2.08	0.03	0.01	0.42	27.05	6.66	0.28	0.20	0.00	0.03	N/A	>100	80.6
ASTM A36 Base Metal	0.16	0.51	0.01	0.02	0.03	0.08	0.06	0.02	0.06	0.00	N/D	N/A	N/A	N/A

N/A = Not Applicable N/D = Not Determined

Martensite boundary at 100% ferrite:

% Ni = 1.036 – ΔNi_{eq} = 1.036 – (–2.07) = 3.106

Martensite boundary at 15.00% Ni_{eq}:

% Ni = 11.50 – ΔNi_{eq} = 11.50 – (–0.21) = 11.71

Step 5. With the % Cr and % Ni values calculated in step 4, and the chosen values for other elements given in step 1, calculate the WRC-1992 chromium equivalents and nickel equivalents for the four options listed above, as follows:

Martensite boundary at 100% ferrite:

WRC Cr_{eq} = % Cr = 25.455

Option 1:

WRC Ni_{eq} =
% Ni + 35x(% C) + 20x(% N)
= 1.036 + 3.5 + 0.4 = 4.936

Option 2:

WRC Ni_{eq} = 2.236 + 3.5 + 0.4 = 6.136

Option 3:

WRC Ni_{eq} = 1.786 + 3.5 + 0.4 = 5.686

Option 4:

WRC Ni_{eq} = 3.106 + 3.5 + 0.4 = 7.006

Martensite boundary at 15.00% Schaeffler Ni_{eq}:

WRC Cr_{eq} = % Cr = 12.296

Option 1:

WRC Ni_{eq} = 11.5 + 3.5 + 0.4 = 15.4

Option 2:

WRC Ni_{eq} = 12.7 + 3.5 + 0.4 = 16.6

Option 3:

WRC Ni_{eq} = 12.25 + 3.5 + 0.4 = 16.15

Option 4:

WRC Ni_{eq} = 11.71 + 3.5 + 0.4 = 15.61

Step 6. Plot the four possibilities for a transposed martensite boundary on the WRC-1992 diagram. The chromium equivalents and nickel equivalents for each option (step 5) provide two points along a transposed martensite boundary. The two points on the WRC-1992 diagram were connected by a straight line, and this line was extrapolated to the upper edge of the diagram to form a martensite boundary.

Figure 2 shows the resulting martensite boundaries transposed from the Schaeffler diagram to the WRC-1992 diagram. The boundaries are fairly close together, and three of the four are parallel. The boundary generated from option 4 (with Schaeffler's variable correction for nitrogen) is not parallel to the other three boundaries.

Experimental Procedure

With four possibilities for a martensite boundary on the WRC-1992 diagram, it is necessary to test the candidates with experimental data. As this required testing of many compositions, a method was devised to obtain numerous deposit compositions from a limited number of filler metals. This consisted of single-pass bead-on-plate welds using the submerged arc process. By varying wire feed speed (current) and, to a certain extent, voltage, it was possible to obtain different dilution levels on mild steel base metal (ASTM A36). In general, increasing the wire feed speed (current) causes increasing dilution, and this is a major effect. In general, increasing the voltage also increases dilution, but the effect is not as strong as that of wire feed speed. Changing from DC electrode positive (DCEP) polarity to DC electrode negative (DCEN) polarity also generally reduces dilution.

Two types of fluxes were used as another means of varying deposit composition with a given wire — highly basic unalloyed flux and acid flux containing considerable free metallic chromium. A highly basic unalloyed flux produces a lower ratio of chromium to nickel, with a particular electrode at a given dilution level, than does a high-chromium flux. Most of the welds with basic flux were made with 880 flux, but another basic flux, 882, was used for a few DCEN welds because this flux offers better welding characteristics with DCEN. The acid high-chromium flux, A-100, welds acceptably with both DCEP and DCEN.

The wires used were all 3/32 in. (2.4 mm) in diameter. Two were standard commercially available solid wires — AWS A5.9 Classes ER308L and ER309L. Nine were laboratory-made, metal-cored wires designed to vary the ratio of chromium to nickel well outside of the normal range available in ER308L or ER309L. Calculated compositions of the metal-cored wires and measured compositions of the solid wires are given in Table 1. Also shown is the composition of two six-layer weld deposits using Wire 119 — one with the basic flux and one with the acid high-chromium flux. It should be noted that the chromium content of the six-layer deposit with the acid high-chromium flux and Wire 119 is about 8% higher than the chromium content of the corresponding deposit with the basic flux. Table 1 includes a representative composition of the ASTM A36 steel base metal used in this program. Not all of the base metal pieces came from the same heat, so there may be very minor differences in composition for some of the test pieces. Since the weld deposit was chemically analyzed, this should not cloud the results.

Evidence of martensite in the deposits was sought in three ways. Magnetic measurements of the deposits were compared with predictions of the Schaeffler and WRC-1992 diagrams. Since both

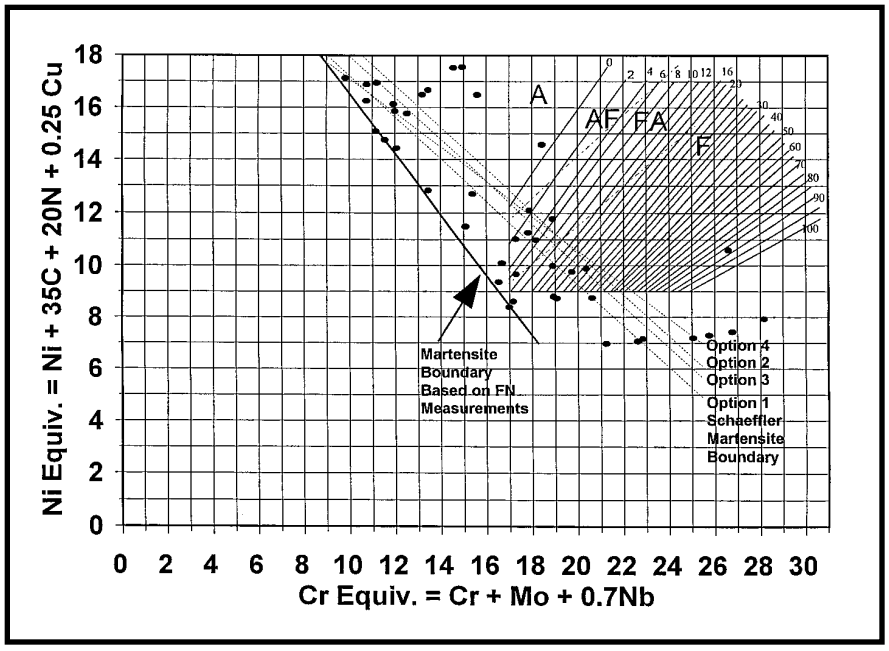

Fig. 6 — WRC-1992 diagram, with compositions having measured FN less than 1.0, or having measured FN less than or equal to the WRC-1992 FN + 1, plotted as solid ellipses. The lower left limit of these points is taken to be the "martensite boundary based on FN measurements."

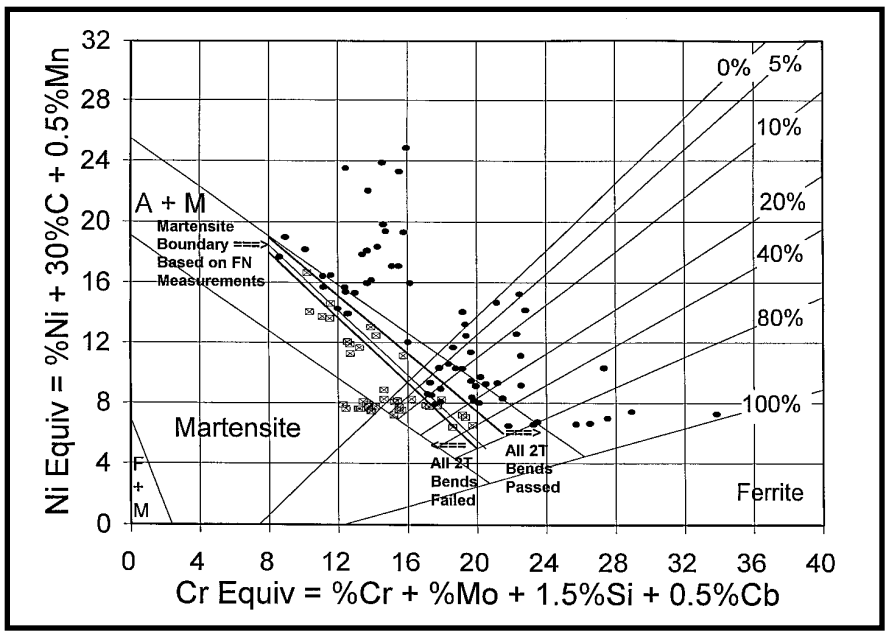

Fig. 7 — Schaeffler diagram, with compositions that passed the 2T bend test indicated as solid ellipses and compositions that failed the 2T bend test indicated as open rectangles.

martensite and ferrite are ferro-magnetic, it is not possible to be absolutely certain which phase (or which proportions of each phase) is responsible for a given magnetic response. Nevertheless, magnetic measurements turn out to be very useful. Second, the longitudinal bend test of each weld deposit was examined for cracking. Cracks occur when the weld has insufficient ductility to pass the bend test, and this is considered to be due to martensite. Third, selected deposits were examined after bending for metallographic evidence of martensite by etched appearance.

The test coupon for martensite determination was an ASME-type longitudinal face bend test. This is normally a bend test in which the bend specimen thickness is twice the bending radius (a 2T bend test) that requires 20% minimum elongation to pass. Martensite makes the weld brittle, resulting in specimen cracks during bending, so this is a go/no-go test that is very quickly executed. Since the A36 base metal was ½-in. (12.7-mm) thick, the bend specimen was bent around a 1-in. (25.4-mm) radius bar. The weld bead reinforcement extends above the surface of the base metal by perhaps 3/32 in. (2.4 mm) to ⅛ in. (3.2 mm), so that the elongation requirement for the weld metal is actually somewhat more than 20%, if the weld is to pass the bend test. Thus, the results should be somewhat conservative. Figure 3 shows two such bend test specimens, one passing the test and one failing the test (as evidenced by transverse cracks after bending). Before bending, the top surface of each weld deposit was lightly ground on a belt sander, with the grinding marks parallel to the length of the specimen, to smooth the surface for ferrite measurement and to prevent surface ripples from influencing the bend test. Cracks found after bending invariably extended completely across the welds, so it could not be determined with certainty the point at which cracking initiated.

A second means of detecting the presence of martensite in some samples was to use a ferrite measuring instrument (Fischer Feritscope Model MP-3), calibrated according to AWS A4.2, before and after bending. Martensite is ferromagnetic, just as is ferrite. If a magnetic response (a "Ferrite Number") was found in a composition above and to the left of the 0 FN line on the WRC-1992 diagram, it could be concluded to be due to martensite, not ferrite. Furthermore, weld deposits that exhibited a magnetic response appreciably higher than the FN predicted by the WRC-1992 diagram could be inferred to contain martensite as well as ferrite. Also, some weld deposits showed an increase in magnetic response as a result of bending, indicating that some martensite was forming during bending. The magnetic response of only a few welds was examined after bending, but almost all of the welds were measured for "Ferrite Number" before bending. Note that "Ferrite Number" or "FN" is used in quotation marks here because the response could be due to ferrite and/or martensite.

After the bend test of each sample was completed, the sample was reverse-bent flat again. Then chips were milled from the weld metal in the vicinity of the former apex of the bend for analysis of carbon, sulfur and nitrogen by fusion methods (given in ASTM E1019). After the chips were removed, the remainder of the weld surface in the vicinity of the apex of the bend was finish-ground to a distance of about 1/32 in. (0.8 mm) above the original base metal surface, and optical emission spectrophotometry (OES, as

Table 2 — Experimental Weld Deposit Compositions, Bend Test Results and Welding Conditions

Weld	Deposit Composition, Weight Percent											Measured	WRC	Schaeffler		Measured FN after	WRC-1992		Schaeffler		Wire Feed	Travel Speed			Stickout	
Number	C	Mn	P	S	Si	Cr	Ni	Mo	Cu	Nb	N	"FN"	FN	% Ferrite	Bend	Bend	Creq	Nieq	Creq	Nieq	ipm	ipm	Volts	Polarity	in.	Flux
119-1	0.087	0.94	0.015	0.010	0.48	13.47	9.41	<0.02	0.05	0.00	0.019	0.6	0.0	0.0	2 cracks	N.D.	13.47	12.85	14.19	12.49	60	11	34	DCEP	1-1/4	880
119-2	0.088	1.12	0.013	0.011	0.47	13.18	9.87	<0.02	0.05	0.00	0.018	6.1	0.0	0.0	2 cracks	N.D.	13.18	13.32	13.89	13.07	90	13-1/2	34	DCEP	1-1/4	880
119-3	0.089	1.05	0.013	0.011	0.46	11.97	8.72	<0.02	0.05	0.00	0.018	29.8	0.0	0.0	cracks	N.D.	11.97	12.21	12.66	11.92	120	18	34	DCEP	1-1/4	880
119-4	0.088	1.01	0.013	0.012	0.42	12.06	8.15	<0.02	0.05	0.00	0.017	29.1	0.0	0.0	cracks	N.D.	12.06	11.58	12.69	11.30	150	22-1/2	34	DCEP	1-1/4	880
119-5	0.088	1.02	0.013	0.012	0.44	12.56	8.55	<0.02	0.05	0.00	0.018	34.8	0.0	0.0	cracks	N.D.	12.56	12.00	13.22	11.70	180	27	34	DCEP	1-1/4	880
119-100-1	0.090	1.70	0.019	0.012	0.47	26.62	6.78	<0.02	0.00	0.00	0.034	18.0	86.7	54.9	ok	N.D.	26.62	10.61	27.33	10.33	60	11	34	DCEP	1-1/4	A-100
119-100-2	0.106	1.35	0.024	0.012	0.55	21.50	8.76	<0.02	0.04	0.00	0.034	12.6	10.7	10.3	ok	N.D.	21.50	13.16	22.33	12.62	90	13-1/2	34	DCEP	1-1/4	A-100
119-100-3	0.090	1.26	0.020	0.013	0.50	18.91	8.06	<0.02	0.05	0.00	0.029	5.4	5.2	7.0	ok	N.D.	18.91	11.80	19.66	11.39	120	18	34	DCEP	1-1/4	A-100
119-100-4	0.091	1.22	0.017	0.014	0.47	17.90	8.38	<0.02	0.05	0.00	0.027	2.0	1.7	2.3	ok	N.D.	17.90	12.12	18.61	11.72	150	22-1/2	34	DCEP	1-1/4	A-100
119-100-5	0.095	1.17	0.015	0.015	0.43	15.09	7.73	<0.02	0.05	0.00	0.022	0.1	0.0	0.0	2 cracks	N.D.	15.09	11.51	15.74	11.17	180	27	34	DCEP	1-1/4	A-100
309-1	0.073	1.26	0.019	0.011	0.50	21.71	8.34	0.11	0.07	0.01	0.050	20.4	18.1	16.2	ok	N.D.	21.83	11.91	22.58	11.16	90	13-1/2	34	DCEP	1-1/4	A-100
309-2	0.080	1.18	0.014	0.012	0.42	18.07	7.33	0.09	0.07	0.00	0.043	5.8	5.0	7.7	ok	N.D.	18.16	11.01	18.79	10.32	120	18	34	DCEP	1-1/4	A-100
309-3	0.090	1.02	0.008	0.014	0.34	14.05	5.07	0.07	0.07	0.00	0.036	62.0	0.0	0.0	cracks	N.D.	14.12	8.96	14.63	8.28	150	22-1/2	34	DCEP	1-1/4	A-100
309-4	0.099	0.97	0.005	0.014	0.29	11.77	4.47	0.06	0.06	0.00	0.031	84.0	0.0	0.0	cracks	N.D.	11.83	8.57	12.27	7.93	180	27	34	DCEP	1-1/4	A-100
309-5	0.090	1.12	0.017	0.014	0.37	15.57	5.03	0.08	0.07	N.D.	0.035	11.8	2.7	6.3	2 cracks	N.D.	15.65	8.90	16.21	8.29	135	20	34	DCEP	1-1/4	A-100
309-6	0.088	1.22	0.017	0.012	0.36	17.76	7.36	0.08	0.07	N.D.	0.041	3.4	3.2	5.7	ok	N.D.	17.84	11.28	18.38	10.61	125	18	34	DCEP	1-1/4	A-100
309-7	0.079	1.22	0.018	0.012	0.35	17.21	7.36	0.08	0.07	N.D.	0.045	2.1	2.3	4.5	ok	N.D.	17.29	11.04	17.82	10.34	130	18	34	DCEP	1-1/4	A-100
309-8	0.095	1.07	0.016	0.013	0.34	12.84	4.73	0.07	0.07	N.D.	0.034	79.8	0.0	0.0	cracks	N.D.	12.91	8.75	13.42	8.12	150	20	32	DCEP	1-1/4	A-100
309-9	0.098	1.06	0.016	0.014	0.32	13.04	4.48	0.07	0.07	N.D.	0.043	79.8	0.0	0.0	cracks	N.D.	13.11	8.79	13.59	7.95	150	20	34	DCEP	1-1/4	A-100
309-10	0.097	1.05	0.016	0.014	0.34	13.12	4.35	0.07	0.07	N.D.	0.033	81.9	0.0	0.0	cracks	N.D.	13.19	8.42	13.70	7.79	150	20	36	DCEP	1-1/4	A-100
309-11	0.099	1.06	0.017	0.014	0.34	13.17	4.19	0.06	0.06	N.D.	0.034	78.0	0.0	0.0	cracks	N.D.	13.23	8.35	13.74	7.69	150	20	38	DCEP	1-1/4	A-100
309-12	0.103	1.05	0.017	0.014	0.33	12.68	4.04	0.06	0.07	N.D.	0.034	82.7	0.0	0.0	cracks	N.D.	12.74	8.34	13.24	7.66	150	20	40	DCEP	1-1/4	A-100
309-13	0.105	1.04	0.017	0.014	0.33	12.57	3.98	0.06	0.07	N.D.	0.033	81.8	0.0	0.0	cracks	N.D.	12.63	8.33	13.13	7.65	150	20	42	DCEP	1-1/4	A-100
309-14	0.101	1.05	0.018	0.014	0.35	13.27	3.94	0.06	0.07	N.D.	0.034	77.0	0.0	0.0	cracks	N.D.	13.33	8.17	13.86	7.50	150	20	44	DCEP	1-1/4	A-100
309-15	0.105	1.07	0.019	0.014	0.35	13.31	3.79	0.06	0.06	N.D.	0.033	78.3	0.0	0.0	cracks	N.D.	13.37	8.14	13.90	7.48	150	20	46	DCEP	1-1/4	A-100
309-16	0.100	1.11	0.020	0.013	0.38	14.87	4.21	0.06	0.07	N.D.	0.041	74.2	1.6	5.5	cracks	N.D.	14.93	8.55	15.50	7.77	150	20	48	DCEP	1-1/4	A-100
309-17	0.096	1.21	0.020	0.011	0.44	18.40	6.81	0.09	0.06	0.00	0.043	54.5	6.2	8.7	ok	N.D.	18.49	11.05	19.15	10.30	120	20	34	DCEP	1-1/4	A-100
309-18	0.093	1.13	0.019	0.013	0.38	14.73	4.82	0.07	0.07	N.D.	0.036	58.3	1.0	2.8	1 crack	N.D.	14.80	8.81	15.37	8.18	120	20	36	DCEP	1-1/4	A-100
309-19	0.095	1.12	0.019	0.013	0.37	14.59	4.67	0.07	0.07	N.D.	0.037	66.5	0.8	2.4	1 crack	N.D.	14.66	8.75	15.22	8.08	120	20	38	DCEP	1-1/4	A-100
309-20	0.099	1.08	0.019	0.013	0.34	13.55	4.29	0.07	0.07	N.D.	0.035	77.5	0.0	0.0	cracks	N.D.	13.62	8.47	14.13	7.80	120	20	40	DCEP	1-1/4	A-100
309-21	0.078	1.22	0.019	0.013	0.41	16.58	6.42	0.08	0.07	N.D.	0.047	2.8	2.7	6.2	ok	N.D.	16.66	10.11	17.28	9.37	100	16	34	DCEP	1-1/4	A-100
309-22	0.085	1.21	0.020	0.013	0.40	17.23	5.79	0.08	0.07	N.D.	0.045	4.6	6.3	9.4	ok	N.D.	17.31	9.68	17.91	8.95	100	16	36	DCEP	1-1/4	A-100
309-23	0.084	1.18	0.020	0.013	0.39	16.47	5.50	0.07	0.07	N.D.	0.046	3.7	4.0	8.1	ok	N.D.	16.54	9.38	17.13	8.61	100	16	38	DCEP	1-1/4	A-100
309-24	0.081	1.27	0.022	0.011	0.44	19.46	6.66	0.09	0.06	0.00	0.044	20.8	13.5	14.2	ok	N.D.	19.55	10.39	20.21	9.73	100	16	40	DCEP	1-1/4	A-100
309-48	0.102	1.10	0.020	0.014	0.38	14.83	3.95	0.06	0.07	N.D.	0.036	72.0	2.0	6.3	cracks	N.D.	14.89	8.26	15.46	7.56	140	20	48	DCEP	1-1/4	A-100
309-120	0.098	1.09	0.020	0.013	0.37	14.56	3.76	0.06	0.06	N.D.	0.038	78.8	2.0	6.4	cracks	N.D.	14.62	7.97	15.18	7.25	120	20	34	DCEP	1-1/4	A-100
309-130	0.100	1.10	0.021	0.013	0.38	15.00	4.01	0.06	0.07	N.D.	0.039	71.5	2.4	6.9	cracks	N.D.	15.06	8.31	15.63	7.56	130	20	48	DCEP	1-1/4	A-100
120-1	0.113	1.17	0.023	0.012	0.58	21.59	11.31	0.02	<0.04	N.D.	0.039	7.5	2.7	4.0	ok	N.D.	21.61	16.05	22.48	15.29	90	13-1/2	34	DCEP	1	A-100
120-2	0.116	1.10	0.018	0.014	0.50	18.60	9.23	<0.02	<0.04	N.D.	0.031	2.3	0.4	0.0	ok	N.D.	18.60	13.91	19.35	13.26	120	18	34	DCEP	1	A-100
120-3	0.122	1.00	0.016	0.014	0.43	15.39	7.89	<0.02	0.04	N.D.	0.027	0.3	0.0	0.0	ok	N.D.	15.39	12.71	16.04	12.05	150	22-1/2	34	DCEP	1	A-100
120-5	0.098	1.30	0.016	0.013	0.51	20.41	11.11	<0.02	0.04	N.D.	0.027	3.6	1.8	1.5	ok	N.D.	20.41	15.09	21.18	14.70	165	24	34	DCEP	1	A-100
120-11	0.083	0.84	0.013	0.010	0.45	11.85	9.17	<0.02	0.05	0.00	0.018	N.D.	0.0	0.0	cracks	N.D.	11.85	12.45	12.53	12.08	90	11	34	DCEP	1	880
121-1	0.107	1.30	0.025	0.012	0.59	21.92	10.34	<0.02	0.04	N.D.	0.033	9.5	6.8	7.5	ok	N.D.	21.92	14.76	22.81	14.20	90	13-1/2	34	DCEP	1	A-100
121-2	0.111	1.15	0.021	0.014	0.53	18.61	8.58	<0.02	0.04	N.D.	0.030	2.9	1.6	2.6	ok	N.D.	18.61	13.08	19.41	12.49	120	18	34	DCEP	1	A-100
121-3	0.113	1.12	0.016	0.014	0.50	18.44	10.12	<0.02	<0.04	N.D.	0.025	0.7	0.0	0.0	ok	N.D.	18.44	14.58	19.19	14.07	150	22-1/2	34	DCEP	1	A-100
121-4	0.122	0.95	0.017	0.015	0.39	14.03	4.75	<0.02	0.04	N.D.	0.028	56.9	0.0	0.0	cracks	N.D.	14.03	9.59	14.62	8.89	180	27	34	DCEP	1	A-100
121-5	0.111	0.91	0.013	0.014	0.30	11.97	3.89	<0.02	0.05	N.D.	0.018	81.2	0.0	0.0	2 cracks	N.D.	11.97	8.15	12.42	7.68	165	24	34	DCEP	1	A-100
308-1	0.053	1.46	0.020	0.013	0.50	18.89	7.15	0.03	0.05	N.D.	0.049	11.6	12.0	13.3	ok	N.D.	18.92	10.00	19.67	9.47	100	16	28	DCEN	1-1/4	A-100
308-2	0.055	1.49	0.024	0.012	0.54	20.35	6.95	0.03	0.05	N.D.	0.050	21.6	21.0	20.4	ok	N.D.	20.38	9.89	21.19	9.35	100	16	34	DCEN	1-1/4	A-100
308-3	0.064	1.48	0.022	0.011	0.54	19.13	6.49	<0.02	0.05	N.D.	0.050	30.4	14.5	16.0	ok	N.D.	19.13	9.74	19.94	9.15	100	16	40	DCEN	1-1/4	A-100
308-4	0.059	1.46	0.022	0.013	0.52	19.71	6.77	0.03	0.05	N.D.	0.046	17.9	17.8	17.7	ok	N.D.	19.74	9.77	20.52	9.27	120	18	34	DCEN	1-1/4	A-100
308-5	0.066	1.35	0.020	0.013	0.47	16.91	5.32	<0.02	0.05	N.D.	0.045	11.4	9.2	12.2	ok	N.D.	16.91	8.54	17.62	7.98	140	20	34	DCEN	1-1/4	A-100
308-6	0.066	1.35	0.020	0.011	0.47	17.16	5.45	0.03	0.05	N.D.	0.043	8.9	10.2	12.8	ok	N.D.	17.19	8.63	17.90	8.11	150	20	34	DCEN	1-1/4	A-100

N.D. = Not Determined

Table 2 — Experimental Weld Deposit Compositions, Bend Test Results and Welding Conditions (Continued)

Weld	Deposit Composition, Weight Percent											Measured	WRC	Schaeffler		Measured FN after	WRC-1992		Schaeffler		Wire Feed	Travel Speed			Stickout	
Number	C	Mn	P	S	Si	Cr	Ni	Mo	Cu	Nb	N	"FN"	FN	% Ferrite	Bend	Bend	Creq	Nieq	Creq	Nieq	ipm	ipm	Volts	Polarity	in.	Flux
308-7	0.070	1.31	0.019	0.012	0.44	16.35	5.14	0.03	0.05	N.D.	0.044	26.5	6.8	10.4	1 crack	N.D.	16.38	8.48	17.04	7.90	160	20	34	DCEN	1-1/4	A-100
308-8	0.067	1.36	0.021	0.013	0.48	16.58	5.83	0.02	0.05	0.00	0.044	9.3	4.6	8.5	ok	86.1	16.60	9.07	17.32	8.52	160	20	36	DCEN	1-1/4	A-100
308-9	0.085	1.36	0.022	0.013	0.47	17.19	5.00	0.03	0.05	0.00	0.043	12.9	9.4	12.3	crack	N.D.	17.22	8.85	17.93	8.23	160	20	38	DCEN	1-1/4	A-100
308-10	0.080	1.29	0.021	0.012	0.46	16.50	4.75	0.03	0.05	0.00	0.039	43.7	8.1	11.5	crack	N.D.	16.53	8.34	17.22	7.80	160	20	40	DCEN	1-1/4	A-100
308-11	0.060	1.42	0.025	0.012	0.51	18.92	5.89	0.04	0.05	0.00	0.041	11.5	18.8	19.4	ok	N.D.	18.96	8.82	19.73	8.40	140	16	36	DCEN	1-1/4	A-100
308-12	0.061	1.38	0.029	0.011	0.51	19.04	5.62	0.04	0.06	0.00	0.049	12.3	19.9	22.3	ok	N.D.	19.08	8.75	19.85	8.14	140	16	38	DCEN	1-1/4	A-100
308-13	0.073	1.28	0.024	0.014	0.47	16.97	5.03	0.02	0.05	0.00	0.041	11.2	10.2	13.2	cracks	N.D.	16.99	8.42	17.70	7.86	140	16	40	DCEN	1-1/4	A-100
308-14	0.060	1.49	0.027	0.010	0.56	20.58	5.78	0.04	0.05	N.D.	0.044	19.8	30.8	32.8	ok	N.D.	20.62	8.77	21.46	8.33	120	14	38	DCEN	1-1/4	A-100
308-15	0.055	1.48	0.029	0.010	0.60	21.63	6.79	0.04	0.05	N.D.	0.045	34.5	32.8	31.2	ok	N.D.	21.67	9.63	22.57	9.18	120	14	40	DCEN	1-1/4	A-100
308-16	0.076	1.31	0.025	0.012	0.51	19.29	5.11	0.03	0.05	0.00	0.040	49.0	22.3	24.5	ok	N.D.	19.32	8.58	20.09	8.05	120	14	42	DCEN	1-1/4	A-100
65N1693-1	0.114	1.38	0.024	0.011	0.37	15.42	11.90	0.18	0.19	N.D.	0.028	0.3	0.0	0.0	ok	N.D.	15.60	16.50	16.16	16.01	100	12	32	DCEP	1-1/4	880
65N1693-2	0.111	1.36	0.024	0.011	0.36	14.78	13.10	0.17	0.19	N.D.	0.027	0.4	0.0	0.0	ok	N.D.	14.95	17.57	15.49	17.11	120	14	32	DCEP	1-1/4	880
65N1693-3	0.108	1.34	0.023	0.013	0.36	14.40	13.21	0.17	0.19	N.D.	0.025	0.5	0.0	0.0	ok	N.D.	14.57	17.54	15.11	17.12	140	16	32	DCEP	1-1/4	880
65N1693-4	0.115	1.29	0.022	0.015	0.32	13.02	11.91	0.16	0.18	N.D.	0.026	0.3	0.0	0.0	ok	N.D.	13.18	16.50	13.66	16.01	160	18	32	DCEP	1-1/4	880
65N1693-5	0.117	1.33	0.022	0.014	0.31	13.30	12.02	0.16	0.17	N.D.	0.026	0.3	0.0	0.0	ok	N.D.	13.46	16.68	13.93	16.20	180	20	32	DCEP	1-1/4	880
65N1693-6	0.113	1.29	0.020	0.012	0.29	12.39	11.30	0.14	0.17	0.00	0.024	0.2	0.0	0.0	ok	N.D.	12.53	15.78	12.97	15.34	200	20	32	DCEP	1-1/4	880
65N1693-7	0.118	1.20	0.018	0.013	0.25	10.59	9.64	0.12	0.15	0.00	0.021	10.9	0.0	0.0	crack	N.D.	10.71	14.23	11.09	13.78	250	25	36	DCEP	1-1/4	880
65N1694-1	0.123	1.47	0.024	0.012	0.39	15.21	20.47	0.17	0.19	N.D.	0.028	0.9	0.0	0.0	ok	N.D.	15.38	25.38	15.97	24.90	100	12	32	DCEP	1-1/4	880
65N1694-2	0.108	1.42	0.023	0.013	0.36	14.85	19.34	0.16	0.18	N.D.	0.028	0.5	0.0	0.0	ok	N.D.	15.01	23.73	15.55	23.29	120	14	32	DCEP	1-1/4	880
65N1694-3	0.111	1.35	0.024	0.013	0.34	13.94	15.85	0.17	0.18	N.D.	0.026	0.5	0.0	0.0	ok	N.D.	14.11	20.30	14.62	19.86	140	16	32	DCEP	1-1/4	880
65N1694-4	0.121	1.40	0.022	0.014	0.34	13.89	19.57	0.16	0.17	N.D.	0.024	0.4	0.0	0.0	ok	N.D.	14.05	24.33	14.56	23.90	160	18	32	DCEP	1-1/4	880
65N1694-5	0.121	1.37	0.021	0.013	0.31	13.16	17.71	0.15	0.17	N.D.	0.025	0.3	0.0	0.0	ok	N.D.	13.31	22.49	13.78	22.03	180	20	32	DCEP	1-1/4	880
65N1694-6	0.106	1.22	0.020	0.012	0.29	10.99	10.86	0.15	0.17	0.01	0.024	0.2	0.0	0.0	crack	N.D.	11.15	15.09	11.58	14.65	200	20	32	DCEP	1-1/4	880
65N1694-7	0.122	1.19	0.017	0.014	0.26	9.70	12.42	0.11	0.14	0.00	0.021	0.1	0.0	0.0	crack	N.D.	9.81	17.15	10.20	16.68	250	25	36	DCEP	1-1/4	880
65N1695-1	0.106	1.33	0.026	0.014	0.37	15.07	15.49	0.18	0.19	N.D.	0.026	0.6	0.0	0.0	ok	N.D.	15.25	19.77	15.81	19.34	100	12	32	DCEP	1-1/4	880
65N1695-2	0.108	1.28	0.024	0.013	0.35	13.60	14.50	0.17	0.18	N.D.	0.026	0.5	0.0	0.0	ok	N.D.	13.77	18.85	14.30	18.38	120	14	32	DCEP	1-1/4	880
65N1695-3	0.112	1.33	0.024	0.015	0.36	14.04	15.40	0.17	0.18	N.D.	0.027	0.7	0.0	0.0	ok	N.D.	14.21	19.91	14.75	19.43	140	16	32	DCEP	1-1/4	880
65N1695-4	0.111	1.28	0.023	0.013	0.32	13.02	14.15	0.16	0.17	N.D.	0.025	0.3	0.0	0.0	ok	N.D.	13.18	18.58	13.66	18.12	160	18	32	DCEP	1-1/4	880
65N1695-5	0.119	1.31	0.022	0.015	0.30	12.81	13.66	0.15	0.17	N.D.	0.025	0.3	0.0	0.0	ok	N.D.	12.96	18.37	13.41	17.89	180	20	32	DCEP	1-1/4	880
65N1695-6	0.106	1.17	0.019	0.013	0.28	11.05	12.76	0.14	0.16	0.01	0.022	0.1	0.0	0.0	ok	N.D.	11.20	16.95	11.62	16.53	200	20	32	DCEP	1-1/4	880
65N1695-7	0.116	1.19	0.019	0.013	0.26	10.64	12.37	0.12	0.15	0.00	0.021	0.0	0.0	0.0	ok	N.D.	10.76	16.89	11.15	16.45	250	25	36	DCEP	1-1/4	880
65N1716-1	0.110	1.18	0.020	0.016	0.32	11.77	11.83	0.15	0.17	0.00	0.021	0.0	0.0	0.0	ok	N.D.	11.92	16.14	12.40	15.72	160	18	34	DCEP	1-1/4	880
65N1716-2	0.118	1.15	0.019	0.019	0.28	10.60	11.63	0.14	0.15	0.00	0.023	0.0	0.0	0.0	ok	N.D.	10.74	16.26	11.16	15.75	200	20	34	DCEP	1-1/4	880
65N1716-2R	0.112	1.09	0.022	0.018	0.32	11.92	10.05	0.15	0.16	0.00	0.022	0.1	0.0	0.0	ok	37.1	12.07	14.45	12.55	13.96	200	20	34	DCEP	1-1/4	880
65N1716-3	0.116	1.14	0.018	0.021	0.26	9.81	10.02	0.13	0.15	0.00	0.021	N.D.	0.0	0.0	crack	N.D.	9.94	14.54	10.33	14.07	240	22	34	DCEP	1-1/4	880
65N1716-3R	0.118	1.12	0.020	0.018	0.26	10.99	9.54	0.13	0.14	0.00	0.022	12.2	0.0	0.0	cracks	44.5	11.12	14.15	11.51	13.64	240	22	34	DCEP	1-1/4	880
65N1716-4	0.112	1.16	0.019	0.018	0.30	11.40	10.34	0.14	0.16	N.D.	0.023	0.0	0.0	0.0	ok	N.D.	11.54	14.76	11.99	14.28	220	18	34	DCEP	1-1/4	880
65N1716-4R	0.111	1.14	0.022	0.018	0.30	11.86	11.51	0.14	0.15	0.00	0.022	0.0	0.0	0.0	ok	4.5	12.00	15.87	12.45	15.41	220	18	34	DCEP	1-1/4	880
65N1717-1	0.109	1.21	0.019	0.015	0.33	11.83	19.65	0.15	0.17	0.01	0.022	0.0	0.0	0.0	ok	N.D.	11.99	23.95	12.48	23.53	160	18	34	DCEP	1-1/4	880
65N1717-2	0.122	1.05	0.016	0.018	0.26	8.44	14.83	0.11	0.13	0.00	0.019	0.0	0.0	0.0	ok	N.D.	8.55	19.51	8.94	19.02	200	20	34	DCEP	1-1/4	880
65N1717-3	0.122	1.03	0.016	0.018	0.24	8.15	13.56	0.10	0.13	0.00	0.018	0.0	0.0	0.0	ok	N.D.	8.25	18.22	8.61	17.74	240	22	34	DCEP	1-1/4	880
65N1717-4	0.125	1.06	0.017	0.017	0.26	9.62	13.93	0.11	0.14	0.00	0.019	0.0	0.0	0.0	ok	N.D.	9.73	18.72	10.12	18.21	280	20	40	DCEP	1-1/4	880
65N1743-1	0.074	1.51	0.022	0.010	0.50	18.23	4.28	0.15	0.15	0.00	0.043	79.8	21.4	25.6	cracks	N.D.	18.38	7.77	19.13	7.26	60	11	34	DCEP	1	882
65N1743-2	0.074	1.56	0.021	0.011	0.43	18.55	4.09	0.14	0.14	0.00	0.049	82.4	23.9	29.5	cracks	N.D.	18.69	7.70	19.34	7.09	60	11	34	DCEN	1	882
65N1743-3	0.061	1.81	0.041	0.008	0.60	32.75	4.56	0.18	0.18	0.02	0.056	87.3	>100	98.3	ok	N.D.	32.94	7.86	33.84	7.30	60	11	34	DCEP	1	A-100
65N1743-4	0.080	1.47	0.034	0.011	0.51	25.60	3.54	0.14	0.14	0.01	0.047	86.9	>100	86.7	ok	N.D.	25.75	7.32	26.51	6.68	60	11	34	DCEN	1	A-100
65N1743-5	0.087	1.60	0.029	0.012	0.51	28.00	4.02	0.16	0.15	N.D.	0.043	80.2	>100	87.9	ok	N.D.	28.16	7.96	28.93	7.43	90	12	34	DCEP	1	A-100
65N1743-6	0.082	1.42	0.027	0.011	0.45	24.90	3.47	0.14	0.14	N.D.	0.042	75.0	>100	85.2	ok	N.D.	25.04	7.22	25.72	6.64	90	12	34	DCEN	1	A-100
65N1743-7	0.072	1.53	0.028	0.010	0.51	26.60	4.09	0.16	0.16	N.D.	0.040	76.6	>100	87.1	ok	N.D.	26.76	7.45	27.53	7.02	120	15	34	DCEP	1	A-100
65N1743-8	0.085	1.35	0.025	0.011	0.41	22.50	3.38	0.13	0.13	N.D.	0.035	70.4	>100	80.0	ok	N.D.	22.63	7.09	23.25	6.61	120	15	34	DCEN	1	A-100
65N1743-9	0.079	1.46	0.024	0.012	0.41	22.70	3.66	0.15	0.14	N.D.	0.036	73.8	>100	79.2	ok	N.D.	22.85	7.18	23.47	6.76	150	18	34	DCEP	1	A-100
65N1743-10	0.086	1.35	0.023	0.012	0.37	21.10	3.27	0.13	0.13	N.D.	0.034	68.7	>100	64.7	ok	N.D.	21.23	6.99	21.79	6.53	150	18	34	DCEN	1	A-100
65N1743-11	0.085	1.33	0.021	0.013	0.32	19.10	3.38	0.13	0.13	N.D.	0.033	50.3	39.7	42.2	cracks	75.7	19.23	7.05	19.71	6.60	180	21	34	DCEP	1	A-100
65N1743-12	0.091	1.28	0.021	0.014	0.31	18.00	3.07	0.11	0.12	N.D.	0.031	57.2	25.6	31.7	cracks	N.D.	18.11	6.91	18.58	6.44	180	21	34	DCEN	1	A-100

N.D. = Not Determined

described in ASTM E1086) was used to analyze for Mn, P, Si, Cr, Ni, Mo, Nb and Cu. Many of the chip samples were also analyzed for Ni and Cr by wet laboratory methods (given in ASTM E353) to check on the accuracy of the OES results. In general, the two methods of Cr and Ni analysis agreed well. When both methods were used, the wet analysis result is reported herein. With the chemical analysis data, the chromium equivalent and nickel equivalent of each deposit could be plotted on the WRC-1992 diagram, with a different symbol for welds that passed the bend test vs. welds that cracked during bending.

After OES chemical analysis, selected OES samples were cross sectioned in the vicinity of the apex of the bend and were examined metallographically for evidence of martensite. A variety of etches were tried to reveal martensite. Vilella's etch, commonly used for revealing martensite in 12% Cr stainless steels, was only somewhat successful, as many of the welds were rather highly alloyed and would not etch. The etch that was found to be most successful in revealing martensite in all welds so examined was diluted Kane's etch. Kane's etch consists of a solution of 6 g $CuCl_2$, 60 mL of HCl and 6 mL of distilled water. This was diluted with an equal volume of water to make it less aggressive. The sample was immersed for 5 to 10 s. The etch darkens martensite, outlines ferrite and leaves austenite untouched.

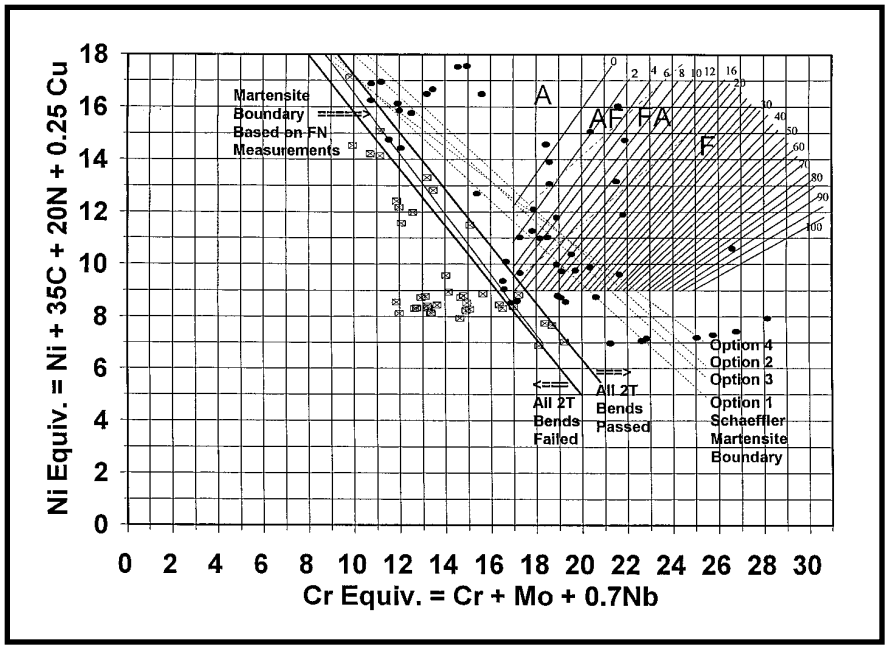

Fig. 8 — WRC-1992 diagram, with compositions that passed the 2T bend test indicated as solid ellipses and compositions that cracked indicated as open rectangles. The two heavy diagonal lines bound the region of compositions of mixed bending behavior — some bent and some broken.

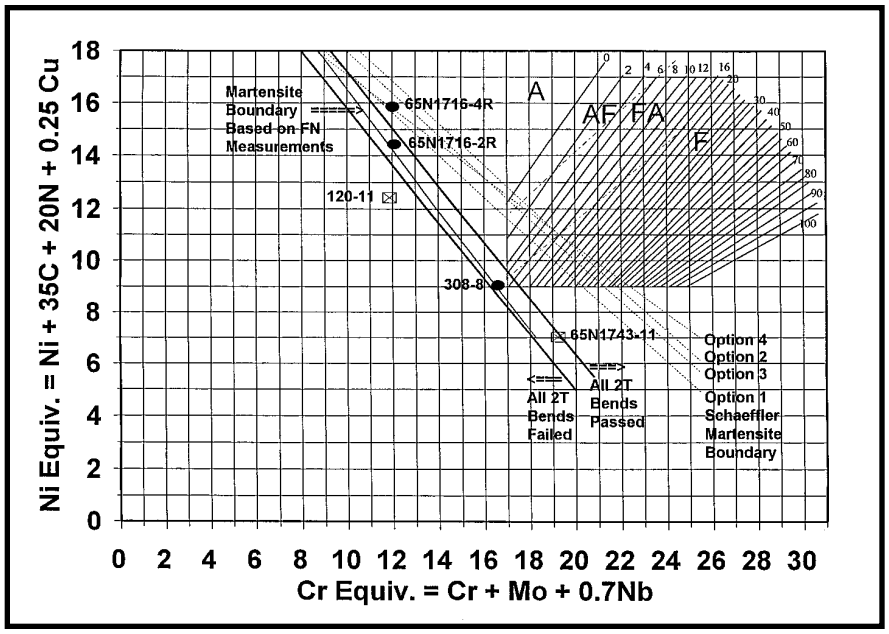

Fig. 9 — WRC-1992 diagram showing locations of compositions examined for microstructure.

Experimental Results

In all, more than 100 deposits were prepared and tested. For each deposit, the deposit composition, calculated chromium and nickel equivalents, calculated and measured "ferrite" content, bend test result and welding conditions to produce the deposit are all listed in Table 2. Welds in Table 2 that have the same prefix were made with the same wire (see Table 1), with composition changes from one deposit to the next due to varying dilution and, sometimes, to varying flux.

Magnetic Measurements

The magnetic measurements of ferrite in Table 2 provide a means of assessing whether martensite is present. First, it should be recognized that welds containing neither ferrite nor martensite can have a trace magnetic response. This can be seen especially well in the data for samples 65N1694-1 through -5. These welds are high enough in nickel (15 to more than 20%) and chromium (13 to 15%) to be fully austenitic; yet they produce magnetic response equivalent to 0.3–0.9 FN. It is a common experience with fully austenitic weld metals, such as Type 310 (nominally 25% Cr, 20% Ni), to also find trace magnetic response, so this did not come as a surprise. This leads to the conclusion that any weld deposit that measured less than 1 "FN" in the as-deposited condition must be at the upper edge of, or above, the range of compositions in either the Schaeffler or WRC-1992 diagram, where martensite is to be found. Therefore, a line along the lower left edge of the area (where these compositions of less than 1 measured "FN") should define part of the martensite boundary, in the area of the diagram where ferrite is not considered to exist.

The remainder of the martensite boundary in either diagram will pass

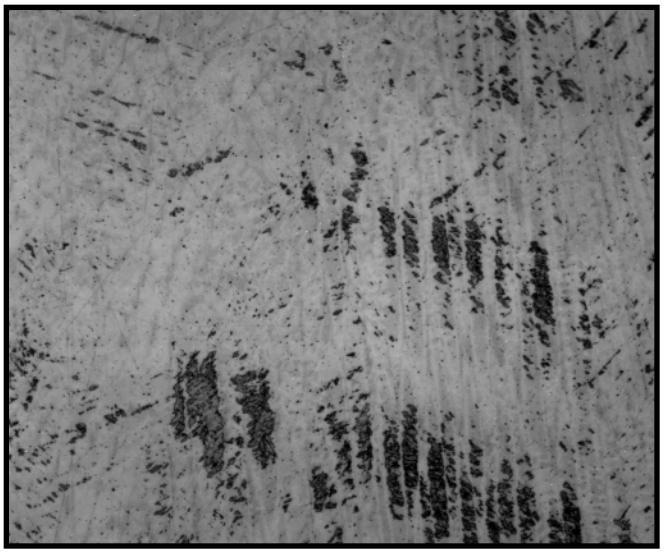

Fig. 10 — Microstructure of weld 65N1716-4R after bending. Diluted Kane's Etch, X200. Magnetic response equal to that of 0 FN before bending and 4.5 FN after bending indicates a small amount of martensite formation during bending. The dark etching regions contain some martensite. No ferrite is present.

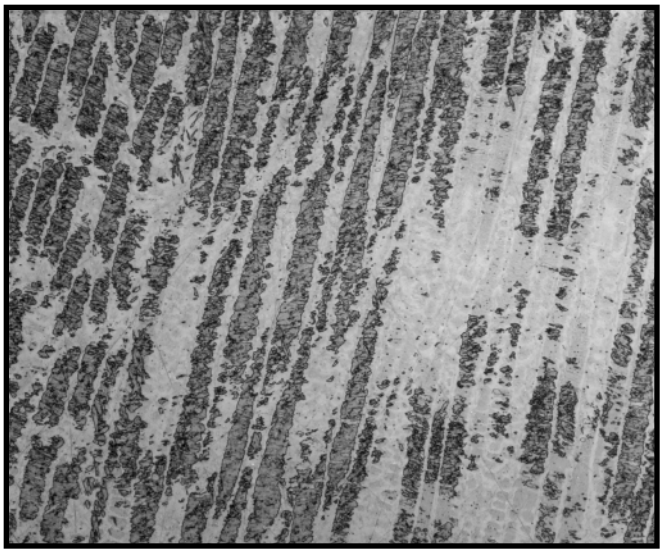

Fig. 11 — Microstructure of weld 65N1716-2R after bending. Diluted Kane's Etch, X200. Magnetic response equal to that of 0.05 FN before bending and 37.1 FN after bending indicates that considerable martensite formed during bending. The dark etching regions contain some martensite. No ferrite is visible.

through composition ranges where ferrite is present. In this region of either diagram, it can be considered that, if the predicted FN from the WRC-1992 diagram agrees well with the measured FN, or if the predicted FN is appreciably higher than the measured FN, then the measured magnetic response is probably due only to ferrite, not to martensite. This would allow the magnetic measurement data to extend the martensite boundary from the fully austenitic composition range into the composition range where some ferrite is also present. First, however, it is appropriate to examine how well the WRC-1992 diagram predicts measured ferrite for the experimental weld deposits. This examination is done only for weld deposits that passed the bend test, so that little or no martensite could be expected to be present to influence the results. The WRC-1992 Ferrite Numbers (calculated with the *Ferrite Predictor* software) are plotted against the measured "Ferrite Numbers," for successful bends only, in Fig. 4. There are two types of data points plotted: Compositions within the region of isoferrite number lines in the WRC-1992 diagram are plotted as solid elliptical symbols; and compositions outside the region of iso-ferrite number lines, whose FN the software estimates by extrapolation, are plotted as open triangles. The perfect correlation line is also included. There is reasonable agreement with the perfect correlation line, with a few outliers.

Deposit compositions whose measured FN is less than 1.0 and compositions whose measured FN is less than or equal to the WRC-1992 FN + 1 can then be concluded to be essentially free of martensite. All of the compositions meeting one or the other of these two criteria are plotted in Fig. 5. Note that, in calculating the Schaeffler Ni_{eq}, nitrogen was ignored, as in option 1, when transposing the Schaeffler martensite boundary to the WRC-1992 diagram. If any other option were used, the Schaeffler Ni_{eq} would be reduced somewhat, moving all of the deposit composition points downward. Figure 5 also includes a line that constitutes the lower left boundary of all of these compositions plotted in the diagram. This line is labeled the "martensite boundary based on FN measurements" in Fig. 5. It does not agree very well with the line labeled "upper martensite boundary according to Schaeffler." Its slope is not the same and it is about 1 Ni_{eq} below near the upper left end of the line and about 4 Ni_{eq} below near the lower right end. It should be noted that any of the other three options for dealing with nitrogen in the Schaeffler Ni_{eq} would produce even poorer agreement between the "martensite boundary based on FN measurements" and the "upper martensite boundary according to Schaeffler."

These same compositions can be plotted on the WRC-1992 diagram using the WRC Cr_{eq} and Ni_{eq}. This is done in Fig. 6, and, again, the "martensite boundary based on FN measurements" is drawn as a line representing the lower left limit of compositions meeting one or the other of the two criteria for concluding that the composition is essentially free of martensite. Figure 6 indicates that this "martensite boundary based on FN measurements" does not agree well with any of the four options for transposing Schaeffler's upper martensite boundary. At the upper left end, it is close to options 1 and 4, but at the lower right end, it is nearly 4 Ni_{eq}, or more, below any of the four options.

2T Bend Tests

The second method of examining martensite formation on the Schaeffler and WRC-1992 diagrams is to plot all compositions that failed the 2T bend test with a different symbol than is used to plot all compositions that passed the 2T bend test. This is done on the Schaeffler diagram in Fig. 7, again using no correction for nitrogen. Two heavy lines are drawn on the Schaeffler diagram. The upper of these two lines is the boundary above and to the right of which all compositions tested passed the 2T bend test. The lower of these two lines is the boundary below and to the left of which all compositions tested failed the 2T bend test. Between these two heavy lines in Fig. 7, the 2T bend test produced mixed results — some compositions passed and some failed. It is noteworthy the "martensite boundary based on FN measurements" lies between the two bend test lines. Agreement with Schaeffler's upper martensite boundary is poor.

Similarly, all compositions that passed the 2T bend test are plotted on the WRC-1992 diagram (Fig. 8), with a different symbol than that used to plot all compositions tested that failed the 2T bend test. Again, a heavy line is drawn in the figure to indicate the lower left limit above which all compositions passed.

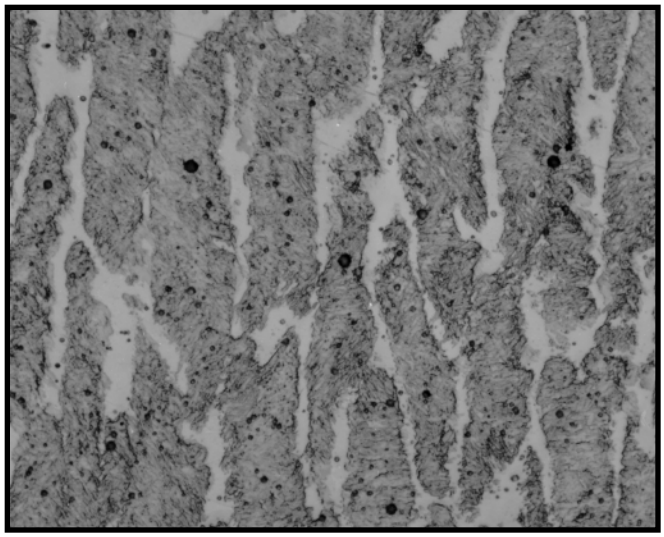

Fig. 12 — Microstructure of weld 120-11 after bending. Diluted Kane's Etch, X500. Magnetic response was not determined before bending the sample, nor before discarding it. The dark etching regions contain some martensite. The light etching regions are austenite. No ferrite is visible.

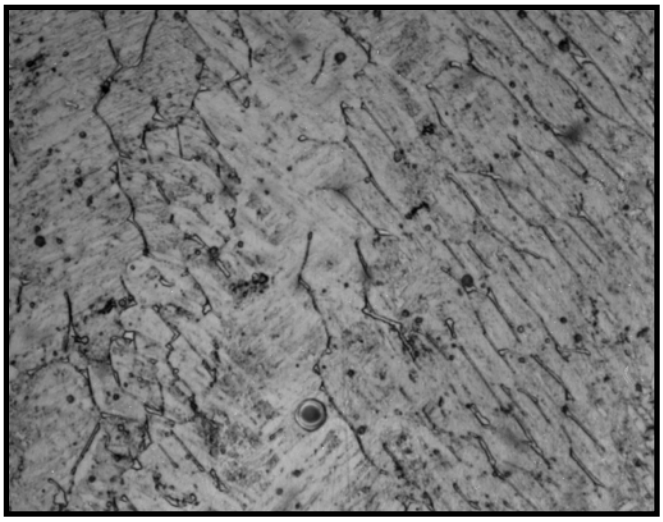

Fig. 13 — Microstructure of weld 308-8 after bending. Diluted Kane's Etch, X1000. Magnetic response equal to that of 9.3 FN before bending, and 86.1 FN after bending, indicates that considerable martensite formed during bending. Ferrite appears as thin elongated islands. Martensite etches more darkly within the austenite matrix.

And a second heavy line is drawn to indicate the upper right limit below which all compositions tested failed the 2T bend test. Between these two lines is a narrow band of compositions, some of which passed the 2T bend test and some of which failed. The width of this band of compositions having uncertain bending behavior is about 1.4 Cr_{eq} in the horizontal direction, or about 1.4 Ni_{eq} in the vertical direction. Note also that the "martensite boundary based on FN measurements" lies between these two lines, just as it did on the Schaeffler diagram. Agreement with any of the transposed martensite boundaries from the Schaeffler diagram is poor.

Microstructures

The third way to observe martensite is to examine selected weld metal microstructures. Not enough metallographic examination was done to define a martensite boundary based solely on this evidence, but the results serve to corroborate the magnetic and bending findings. Five compositions are chosen for this examination. The first is a composition (65N1716-4R) with calculated FN = 0, which lies in the range where all compositions passed the 2T bend test and are above the "martensite boundary based on FN measurements." The second is a composition (65N1716-2R) with calculated FN = 0, which lies in the range of compositions where some passed (including this one) and some failed the 2T bend test. The third is a composition (120-11) with calculated FN = 0, which lies in the range where all compositions failed the 2T bend test. These first three compositions provide a transition across the martensite boundary region at nearly constant Cr_{eq}, without likelihood of finding any ferrite. The fourth composition (308-8), like the second, lies in the range of compositions in which some (including this one) passed the 2T bend test and some failed, but extrapolation of the iso-ferrite lines in the WRC-1992 diagram results in the expectation that this composition would contain some ferrite (4.6 FN, Table 2). The fifth composition (65N1743-11) also lies in the range of compositions in which some passed the bend test and some (including this one) failed, and extrapolation of the iso-ferrite lines results in the expectation that this composition would contain considerable ferrite (39.7 FN). Figure 9 isolates these five compositions on the WRC-1992 diagram.

Figure 10 shows the microstructure of Weld 65N1716-4R (WRC-1992 Cr_{eq} = 12.00, Ni_{eq} = 15.84), which passed the bend test. It can be seen in Fig. 9 that this combination of Cr_{eq} and Ni_{eq} lies virtually on the transposed Schaeffler martensite lines using option 1 or 4, but below the transposed martensite lines using option 2 or 3. Before bending, this weld showed no magnetic response (0.0 FN), indicating that it was free of martensite at that time. But after bending (and straightening), its magnetic response was equal to 4.5 FN, which indicates that a small amount of martensite formed during bending. The photomicrograph of Fig. 10 shows small patches of dark-etching martensite (which include some remnant austenite) in an austenite matrix. The martensitic areas seem to be concentrated in dendrite cores, which would be expected to be leaner in alloying elements than the interdendritic spaces, and therefore could be expected to transform to martensite first. This observation of a small amount of martensite after bending, taken together with the magnetic response in this sample equivalent to 4.5 FN after bending, indicates clearly that the magnetic method of detecting martensite is quite sensitive.

Figure 11 shows the microstructure of Weld 65N1716-2R (WRC-1992 Cr_{eq} = 12.07, Ni_{eq} = 14.41), which also passed the bend test. With lower Ni_{eq} than the weld of Fig. 10, but virtually the same Cr_{eq}, this composition lies below all of the transposed Schaeffler martensite boundaries in Fig. 9. Its composition lies within the band of compositions in which some passed the bend test and some failed the bend test. This deposit passed the bend test. As deposited, its magnetic response was equal to that of 0.05 FN, indicating that there was virtually no martensite present. But after bending, the magnetic response was equal to that of 37.1 FN, so a great deal of martensite formed during bending. Figure 11 shows the extensive martensite-containing regions, concentrated in dendrite cores.

Figure 12 shows the microstructure of Weld 120-11 (WRC-1992 Cr_{eq} = 11.85, Ni_{eq} = 12.44), which cracked in the bend test. This weld has virtually the same Cr_{eq} as that of the two previously examined welds, but its Ni_{eq} is lower. It lies in the region in Fig. 9 in which all of the samples cracked during bending. Figure 12 shows that this deposit is very heavily

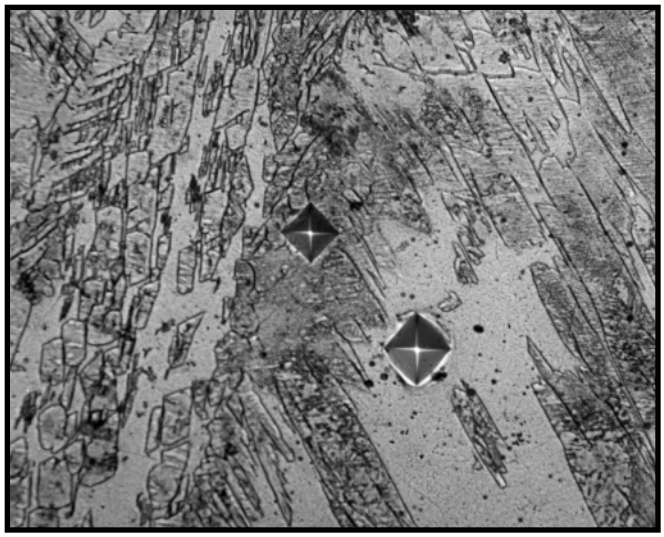

Fig. 14 — Microstructure of weld 65N43-11 after bending. Diluted Kane's Etch, X500. Magnetic response equal to that of 50.3 FN before bending and 75.7 FN after bending indicates that some martensite formed during bending. Ferrite appears light, while martensite in austenite appears dark. Vickers hardness impressions measured 430 in the martensite-containing regions, 320 in the ferrite.

martensitic. Unfortunately, this sample was discarded without evaluating magnetic response. Taken together, Figs. 10–12 provide a spectrum of microstructures at about 12 Cr_{eq} with decreasing Ni_{eq} making a transition from no martensite as deposited to very high martensite, all with no ferrite in the microstructure.

Weld deposits containing ferrite, along with austenite and martensite after bending, were also produced, and it is interesting to examine a few of these. Figure 13 shows the microstructure of Weld 308-8 (WRC-1992 Cr_{eq} = 16.60, Ni_{eq} = 9.06). It lies in the band of compositions in Fig. 9 in which some deposits bent and some cracked during bending. As deposited, its magnetic response was equal to that of 9.3 FN, which is slightly greater than the 4.6 FN the *Ferrite Predictor* software estimates by extrapolating the iso-ferrite lines. After bending, however, its magnetic response was equal to that of 86.1 FN, indicating considerable transformation of austenite to martensite during bending. Nevertheless, it passed the 2T bend test. The microstructure shows thin elongated islands of ferrite and extensive martensite within the austenite matrix.

Figure 14 shows the microstructure of Weld 65N1743-11 (WRC-1992 Cr_{eq} = 19.43, Ni_{eq} = 7.02). It also lies in the band of compositions in Fig. 9 in which some deposits bent and some cracked. As deposited, its magnetic response was equal to that of 50.3 FN, which is a little greater than the 39.7 FN the *Ferrite Predictor* software estimates by extrapolation of the iso-ferrite lines. It should be noted that the higher FN iso-ferrite lines appear to converge when extrapolated toward their lower left, so it is not possible to be sure that all of the magnetic response before bending was due to ferrite — there may have been some martensite present as well. After bending, the magnetic response rose to equal that of 75.7 FN, indicating that some transformation of austenite to martensite occurred during bending. This deposit cracked during bending. Figure 14 shows microhardness impressions in the ferrite and in the martensite. The martensite reading was 430 Vickers, while that of the ferrite was 320 Vickers. No austenite is clearly discernible in Fig. 14, but it is considered that the dark etching areas actually consist of a very fine mixture of martensite and austenite — otherwise, the magnetic response would correspond to well over 100 FN.

Discussion of Results

It has been noted that the measurements of magnetic response lead to a "martensite boundary based on magnetic measurements" that does not agree very well with the upper martensite boundary indicated in Schaeffler's diagram — Fig. 5. This comparison is based upon the assumption that Schaeffler's upper martensite boundary is specific to the as-deposited weld metal (*i.e.*, before bending). It is well known that plastic deformation will induce martensite formation in compositions that are fully austenitic in the annealed condition, such as 304L stainless steel. Hull (Ref. 14) observed deformation-induced martensite in a number of chill cast stainless steels while trying to determine martensite-start temperatures. Deformation was shown to raise the martensite-start temperature. So, as a corollary at ambient temperatures, on the WRC-1992 diagram there would have to be a martensite boundary before bending and a second martensite boundary after bending, at richer compositions than the first martensite boundary (*i.e.*, above and to the right of the first martensite boundary). The present work concentrated on magnetic measurements before bending, with only a few measurements after bending, so it is not possible to propose herein a martensite boundary after bending.

One possibility for explaining the difference between Schaeffler's upper martensite boundary and the "martensite boundary based on magnetic measurements" developed herein is that Schaeffler examined samples that had undergone a small amount of plastic deformation, causing the martensite boundary to be shifted upward as compared to that for deformation-free weld metal. A second possibility is that there was a bias in Schaeffler's chemical analyses and/or in the present chemical analyses. The present analyses were checked by comparing classical wet results with spectrographic results, and NIST standards were used for calibration of all methods used herein. A third possibility is a misinterpretation of when martensite first appears. It is not possible to determine the reason for the difference and it is not proposed to modify the Schaeffler diagram.

It is proposed to modify the WRC-1992 diagram to include a martensite boundary. Figure 6 offers a "martensite boundary based on magnetic measurements" that is appreciably different from any of the four options considered for transposing Schaeffler's upper martensite boundary to the WRC-1992 diagram. The upper left portion of that boundary is rather clear since there is no ferrite to produce possible confounding of the interpretation of magnetic responses. That portion of the boundary is based upon measured FN less than 1.0, but the lower right portion of that boundary is less certain. It is based upon the measured FN being less than or equal to the WRC-1992 calculated FN + 1.0. The problem here is that calculated FN and measured FN cannot be expected to agree exactly. Further, that portion is entirely outside of the region containing iso-ferrite lines in the diagram, so it is necessary to use extrapolated iso-ferrite lines for calculation of the WRC-1992 FN, as was done with the *Ferrite Predictor* software. These extrapolated iso-ferrite lines must be considered as somewhat doubtful because they are beyond the limits of the database used in developing the earlier WRC-1988 diagram (Ref. 15), which is the direct parent of the WRC-1992 diagram.

There is corroborating evidence for the "martensite boundary based on mag-

netic measurements" in the 2T bend test results. Figure 8 shows that this boundary lies in the region in which some bend tests passed and some failed. It is not quite parallel to the two boundaries of that region (the line above and to the right of which all bends passed, and the line below and to the left of which all bends failed), but it is nearly parallel. So the bend test results reflect the magnetic results very well.

It is evident from examination of Fig. 8 that none of the four options for an upper martensite boundary, transposed from the Schaeffler diagram to the WRC-1992 diagram, agrees well with the boundary between experimental compositions that all pass the longitudinal face bend test, and compositions that may or may not pass this test. The transposed boundary from option 1 (which ignores any correction for nitrogen) comes closest to this boundary, but it is overly conservative. That is, if it were used as the basis for accept/reject decisions (rejecting deposit compositions below and to the left of this line), the result would be rejection of a range of compositions that will not contain martensite and that will pass a bend test.

The metallurgist wants to know which compositions will contain martensite. The engineer wants to know whether a bend test can be passed because the ability to pass a bend test is often required in welding procedure qualifications. Both concerns are addressed by the narrow band of compositions included between two lines in Fig. 8 — the line above and to the right of which all compositions passed the 2T bend test, and the line below and to the left of which all compositions failed this bend test. The "martensite boundary based on FN measurements" lies within this region. It must be appreciated that there is a degree of uncertainty in any determination of this sort. The degree of uncertainty in determining a martensite boundary in the WRC-1992 diagram is probably comparable to the width of the region between these two lines. So this region, which includes a degree of uncertainty, is proposed as the upper martensite boundary in the WRC-1992 diagram. For clarity, the WRC-1992 diagram is redrawn in Fig. 15 with only the proposed martensite boundary added. The region to the left of the upper portion of this boundary is labeled "A + M" because both austenite and martensite would be expected in such compositions. Lower and to the left of this boundary, the region is labeled "A + M + F" because deposits could be expected to contain austenite, martensite and ferrite, based upon extrapolation (not shown) of the iso-ferrite lines.

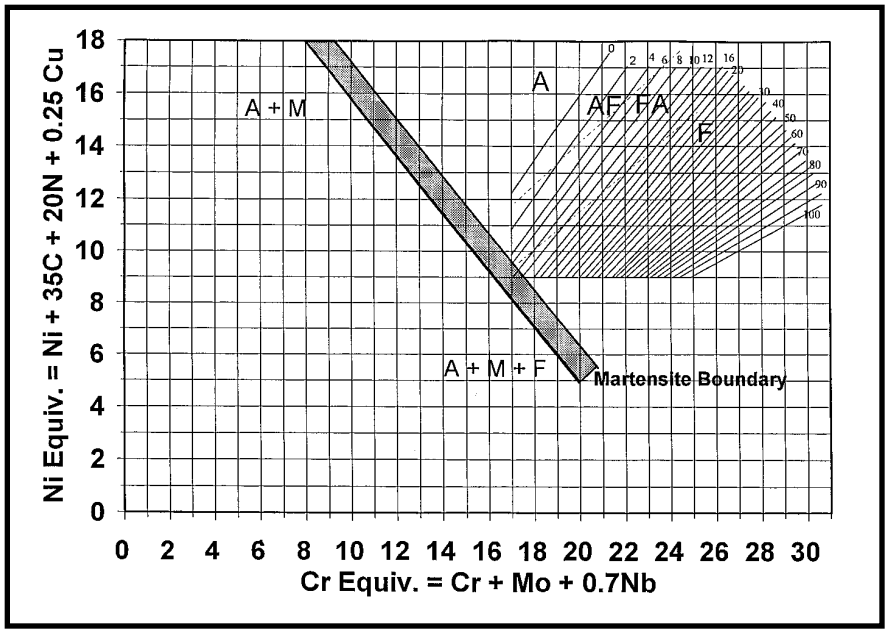

Fig. 15 — WRC-1992 diagram with the martensite boundary for as-deposited weld metal. Compositions below and to the left of the shaded boundary are expected to contain some martensite and to fail an ASME 2T bend test. Compositions above and to the right of the boundary are expected to be free of martensite and to pass an ASME 2T bend test. The behavior of compositions within the boundary is considered to be unpredictable.

It is noteworthy that the magnetic detection limit for martensite and the bend test result boundary coincide rather closely. This seems to say that the presence of martensite before bending is detrimental to bend test performance. But formation of martensite during bending is not detrimental. If the weld deposit is free, or virtually free, of martensite before bending, it will pass the bend test. That should not be surprising — 304 stainless steel often forms some martensite during bending, but bends successfully. If, on the other hand, the weld deposit contains appreciable martensite before bending, it will probably fail the bend test. Note, however, that all of the data herein is for weld deposits of 0.05% C or higher. This was a deliberate choice at the beginning of the program to ensure that martensite formed would be relatively brittle. It is well known that very low carbon martensite (0.03% C or less) can pass the bend test (*e.g.*, Type 410NiMo weld metal). For very low carbon martensite, the prediction of martensite according to the experimental results herein should be correct, but the prediction of bend test failures may not be correct.

Future Work

Since the WRC-1992 diagram does not include manganese in the nickel equivalent, as the Schaeffler and DeLong diagrams did, Fig. 15 has to be interpreted as specific to the manganese level examined herein — about 1% Mn. Szumachowski, *et al.* (Ref. 16), established that there is no effect of manganese on ferrite vs. austenite formation at high temperatures in Cr-Ni stainless steel weld metals. However, Self, *et al.* (Ref. 17), examined the effect of Mn on austenite stability as regards transformation to martensite at low temperatures, and found the effect of Mn to vary with chromium content. In particular, they found Mn to be a more powerful austenite stabilizer at low chromium contents than at high chromium contents. This is being taken into account in further work to extend the examination of martensite appearance to very high Mn weld metals, such as might be obtained from type 307 or 209 welding filler metals.

Conclusions

From results of bend tests of more than 100 compositions, a relatively thin boundary can be drawn on the WRC-1992 diagram shown in Fig. 15, above and to the right of which no martensite would be expected in the as-deposited weld metal and the weld metal would be expected to pass a 2T bend test. Below and to the left of this boundary, martensite can be expected in the weld metal, and it can be expected to fail a 2T bend test. Within the boundary region, results

are expected to be unpredictable. This boundary is appreciably different from any of four possibilities for transposing the upper martensite boundary from the Schaeffler diagram. This boundary is specific to compositions containing approximately 1% Mn.

Acknowledgments

The author is indebted to Peer Reviewers who, on behalf of the AWS Technical Papers Committee, reviewed the original draft of this paper and made a number of insightful comments and suggestions. Their efforts contributed mightily to improving the quality of this final version of the paper. The author is also grateful to The Lincoln Electric Co. for providing the opportunity to pursue this investigation.

References

1. Kotecki, D. J., and Siewert, T. A. 1992. WRC-1992 constitution diagram for stainless steel weld metals: a modification of the WRC-1988 diagram. *Welding Journal* 71(5): 171-s to 178-s.

2. Lefebvre, J. 1993. Guidance on specifications of ferrite in stainless steel weld metal. *Welding in the World* 31(6): 390–407.

3. Kotecki, D. J. 1998. Standards and industrial methods for ferrite measurement. *Welding Journal* 77(5): 49–52.

4. DeLong, W. T. 1974. Ferrite in austenitic stainless steel weld metal. *Welding Journal* 53(7): 273-s to 286-s.

5. Schaeffler, A. L. 1949. Constitution diagram for stainless steel weld metal. *Metal Progress* 56(11): 680–680B.

6. Davis, J. R. 1993. Hardfacing, weld cladding, and dissimilar metal joining. *Metals Handbook*, vol. 6, pp. 817–818.

7. ANSI/AWS A4.2-97, *Standard Procedures for Calibrating Magnetic Instruments to Measure the Delta Ferrite Content of Austenitic and Duplex Ferritic-Austenitic Stainless Steel Weld Metal*. American Welding Society, Miami, Fla.

8. Kotecki, D. J. 1997. Ferrite determination in stainless steel welds — advances since 1974. *Welding Journal* 76(1): 24-s to 37-s.

9. Kotecki, D. J. 1997. FN measurement round robin using shop and field instruments after calibration by secondary standards — summary report. IIW Document II-1318-97. International Institute of Welding, Paris Nord II, France.

10. *Ferrite Predictor* computer software, ©1992, American Welding Institute, Knoxville, Tenn., now distributed by The Lincoln Electric Co. Cleveland, Ohio.

11. *ASME Boiler and Pressure Vessel Code*. 1995. Section III, Division I, Figure NB-2433.1-1. The American Society of Mechanical Engineers, New York, N.Y.

12. Espy, R. H. 1982. Weldability of nitrogen-strengthened stainless steels. *Welding Journal* 61(5): 149-s to 156-s.

13. Schaeffler, A. L. 1991. Private communication.

14. Hull, F. C. 1973. Delta ferrite and martensite formation in stainless steels. *Welding Journal* 52(5): 193-s to 203-s.

15. Siewert, T. A., McCowan, C. N., and Olson, D. L. 1988. Ferrite Number prediction to 100 FN in stainless steel weld metal. *Welding Journal* 67(12): 289-s to 298-s.

16. Szumachowski, E. R., and Kotecki, D. J. 1984. Effect of manganese on stainless steel weld metal ferrite. *Welding Journal* 63(5): 156-s to 161-s.

17. Self, J. A., Matlock, D. K., and Olson, D. L. 1984. An evaluation of austenitic Fe-Mn-Ni weld metal for dissimilar metal welding. *Welding Journal* 63(9): 282-s to 288-s.